A New Structure Model for $Ba_3Nb_2O_8$: A HREM Study

E. García-González, M. Parras, and J. M. González-Calbet*

Departamento de Química Inorgánica, Facultad de Químicas, Universidad Complutense, Madrid-28040, Spain

Received January 4, 2000. Revised Manuscript Received June 5, 2000

The structural investigations performed by powder X-ray diffraction, selected area electron diffraction, and high-resolution electron microscopy on $Ba_3Nb_2O_8$ clearly show that the palmierite structure previously reported for this compound is not adopted. The presence of Nb in the B sublattice induces a change in symmetry from rhombohedral to hexagonal, and a 9H unit cell is formed. The two possible layer stacking sequences, *(ccchhhhhh)* ($P\bar{3}m1$) and *(cchhchhhh)* ($P\bar{3}m1$), are discussed in terms of ordering of both anionic and cationic vacancies.

Introduction

From the ABO_3 cubic perovskite, the change in composition can be brought about by layers of empty octahedra in the center of hexagonal slabs, thus leading to the general formula $A_nB_{n-\delta}O_{3n-x}$ ($\delta \geq 1$, $x \geq 0$). In this sense, the structure type adopted is related to the number of cationic vacancies, and a hh pair (h = hexagonal layer) is required to create an empty site.

When the cationic ratio of A to B is 3:2 ($n = 3$, $\delta = 1$), one of every three B sites remains unoccupied, and different structures can be formed depending on composition and extent of anion deficiency. With $x = 0$ two polytypes can be adopted: the $Cs_3Tl_2O_9$ type where the AO_3 layers are hexagonal close packed and an empty octahedron is situated between face-sharing octahedra,[1] and the 9R-type structure where the stacking sequence is $(hhc)_3$ and a vacant octahedral cavity is located between corner-sharing octahedra. The palmierite structure is derived from that of the 9R polytype when $x = 1$. In this case oxygen-deficient cubic AO_2 layers are formed which forces a change in coordination of the B atoms from octahedral to tetrahedral.

In the Ba−Mo−Nb−O system new compounds have been obtained for the Nb:Mo ratios explored, and the results obtained show the complex crystal chemistry of these phases to be governed by many confluent facts.[2,3] For the A:B::3:2 composition, the structural type adopted ranges from the $Cs_3Tl_2O_9$ type in $Ba_3Mo_2O_9$ to a structure intermediate between the 9R polytype and the palmierite structure for $Ba_3MoNbO_{8.5}$.[2] This new cation-deficient phase was shown to contain an ordered distribution of octahedra and tetrahedra in a 3:2 ratio in the cubic layers of the (hhc) sequence.

Previous work done on $Ba_3Nb_2O_8$[4] showed the compound to crystallize with the palmierite-type structure as the isostoichiometric $Ba_3V_2O_8$. Our structural investigations, however, differ from the results already reported, and the $(hhc)_3$ sequence is not preserved when only Nb occupies the B sublattice.

The present paper describes the results obtained in the structural analysis of $Ba_3Nb_2O_8$. Discussion is made in comparison with the stoichiometrically identical palmierite structure and at the light of the X-ray diffraction, electron diffraction, and high-resolution electron microscopy studies performed.

Experimental Section

The sample of nominal composition $Ba_3Nb_2O_8$ was prepared by the solid-state reaction of $BaCO_3$ (Aldrich, 99.98%) and Nb_2O_5 (Aldrich, 99.5%). Stoichiometric amounts of initial reagents were ground, and the mixture was pressed into a pellet. This pellet was heated at 1250 °C for 96 h. The white homogeneous product was slowly cooled in air (rate, 0.1 °C/min) to room temperature in the platinum crucibles used for the synthesis. It is important to mention that quenching of the product to room temperature led to a partially amorphous material, as shown by X-ray diffraction.

The oxygen content of the sample was determined by thermogravimetric analysis developed on the basis of a CAHN D-200 electrobalance. The sample was reduced under H_2 at 800 °C. The total amount of barium and niobium was determined by inductive coupling plasma (ICP) as well as by EDS X-ray microanalysis carried on a PHILIPS CM20 FEG SuperTwin electron microscope supplied with an EDAX analyzer DX-4, resolution ∼135 eV, and Super Ultra Thin window.

Powder X-ray diffraction was performed on a PHILIPS X'PERT diffractometer equipped with a bent copper monochromator and using Cu Kα radiation.

Selected area electron diffraction (SAED) was carried out on a JEOL 2000FX electron microscope. High-resolution electron microscopy (HREM) was performed on both JEOL 4000EX and PHILIPS CM20 FEG SuperTwin electron microscopes. The samples for electron microscopy were ultrasonically dispersed in 1-butanol and transferred to carbon-coated copper grids.

Results and Discussion

The powder X-ray diffraction pattern revealed a single-phase sample for the nominal composition $Ba_3Nb_2O_8$. The whole pattern could be assigned to a

* To whom correspondence should be addressed.

(1) Mössner, B.; Kemmler-Sack, S. *J. Less-Common Met.* **1985**, *114*, 333.
(2) García-González, E.; Parras, M.; González-Calbet, J. M. *Chem Mater.* **1998**, *10*, 1576.
(3) García-González, E.; Parras, M.; González-Calbet, J. M. *Chem Mater.* **1999**, *11*, 433.
(4) Kemmler-Sack, S.; Treiber, U.; Fadini, A. *Z. Anorg Allg. Chem.* **1979**, *453*, 157.

10.1021/cm000007f CCC: $19.00
Published on Web 08/04/2000

hexagonal lattice of cell parameters $a = 5.82$ Å and $c = 21.15$ Å. These results surprisingly differ from what would be expected. As we comment in the Introduction, $Ba_3V_2O_8$ crystallizes with the palmierite-type structure, and $Ba_3MoNbO_{8.5}$ presents a rhombohedral unit cell derived from the 9R polytype, where the flexibility of the $(hhc)_3$ sequence allows the formation of a modulated structure by introducing mixed $BaO_{2.6}$ cubic layers in the 9R polytype. The presence of Nb in the B sublattice, however, does not stabilize the rhombohedral symmetry of the $(hhc)_3$ sequence, and the unit cell becomes hexagonal.

From the average value of the distance between BaO_3 layers, 2.2−2.3 Å, the cell dimensions are consistent with a nine-layer stacking of close-packed BaO_3 layers. For a 9H type, there are a total of six possible stacking sequences. Three of them correspond to the $P\bar{3}m1$ space group, *(cccccchcch)*, *(hchcchhcc)*, and *(ccchhhhhh)* [(6)-(3), (2)3(1)3, and (4)11(1)11 in the Zhdanov notation],[5] and the other three correspond to the noncentrosymmetric space group $P3m1$, *(cccchchhh)*, *(ccchchchh)* and *(cchhchhhh)* (5211, 4221, 312111). Since the unit cell has to allocate three cationic vacancies, those sequences containing isolated *h* layers seem to be less probable if we consider, as it was mentioned in the Introduction, that the hexagonal cation-deficient perovskite-like oxides stabilize structures which contain at least two consecutive *h* layers. Nevertheless, the six 9H polytypes are in agreement with the unit cell derived from the X-ray diffraction data, and all of them are consistent with the absence of diffraction conditions.

To elucidate the layer sequence of the structure, an electron microscopy study was performed. Figure 1a−c shows the SAED patterns of $Ba_3Nb_2O_8$ taken along the [100], [1$\bar{1}$0], and [001] zone axes. In the latter, the reflections are distributed in a hexagonal array corresponding to a lattice parameter close to 5.8 Å. Besides, the (100) and (1$\bar{1}$0) reciprocal planes also correspond to a hexagonal symmetry, all diffraction maxima being indexed on the previously defined unit cell. The three most relevant zone axes are then in agreement with the above symmetry as well as the absence of systematic extinctions.

The most informative high-resolution images are those taken along the close-packed directions of the layers. Moreover, in the [100] zone the structure is viewed along the Ba−O−Ba rows, and thus, the projected image directly reveals the stacking sequence. The HREM image of $Ba_3Nb_2O_8$ in this projection is shown in Figure 2, where the bright dots can be understood as the image of the O−Ba−O−Ba columns. At this point, it is worth mentioning that the particular morphology of crystallites in this sample difficults its observation in the electron microscope. Crystallites appear as very thick particles where the thin edge does not go over more than a few angstroms.

From the observed contrast, the array of Ba atoms can be interpreted on the basis of only two possibilities of the six 9H existing stacking sequences: *(ccchhhhhh)*, S.G. $P\bar{3}m1$ or *(cchhchhhh)*, S.G. $P3m1$. In addition, these are the only two possibilities if we keep in mind the fact that there are three cationic vacancies in the unit cell.

(5) Zhdanov, G. S. *Dokl. Akad. Nauk. SSSR* **1945**, *48*, 40.

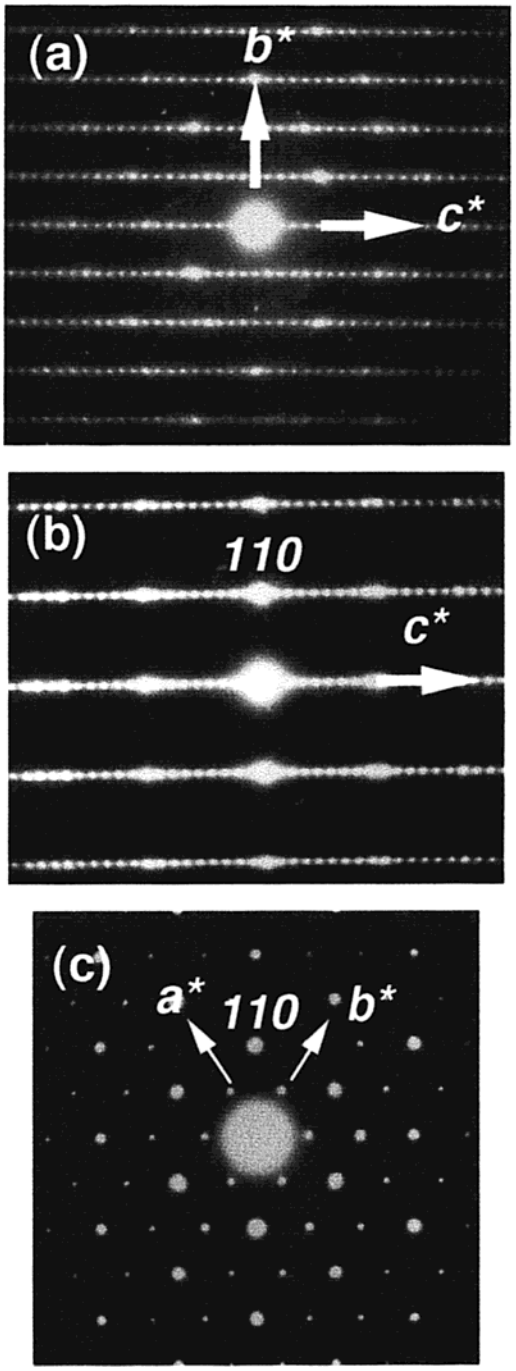

Figure 1. SAED patterns of $Ba_3Nb_2O_8$ taken along the (a) [100], (b) [1$\bar{1}$0], and (c) [001] zone axes.

From the topological point of view, both unit cells differ only in the presence or not of one cubic layer "breaking" the block constituted by the six hexagonal layers. Figure 3a,b shows the ideal structural models in the [100] projection, corresponding to the sequences *(cchhchhhh)* (a) and *(ccchhhhhh)* (b). In the following discussion we will refer to them as models 1 and 2, respectively. The previous statement about the need of two consecutive *h* layers to accommodate the cationic deficiency would be reinforced when any of the two polytypes being adopted.

To make the image analysis easier, we have divided the unit cell into two blocks A and B (see Figure 2) and carefully examined the contrast inside them. The constitution of the two blocks is schematically shown in

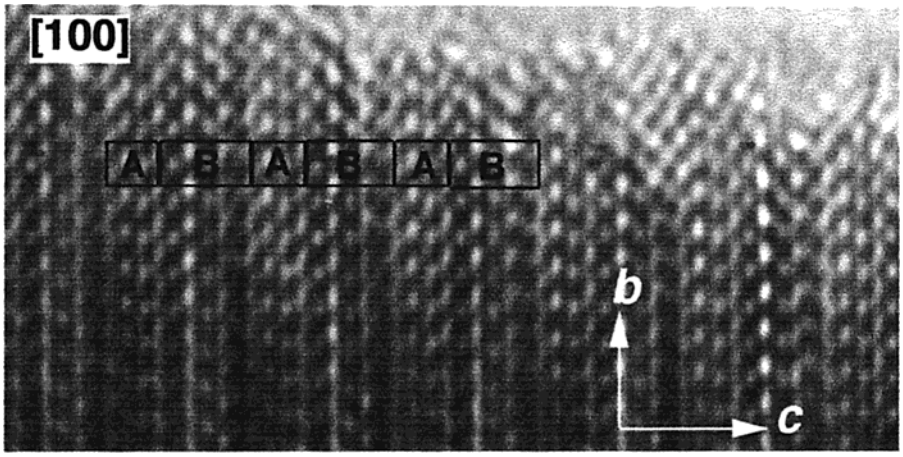

Figure 2. High-resolution electron micrograph of $Ba_3Nb_2O_8$ in the [100] projections. Blocks constituting the unit cell have been drawn.

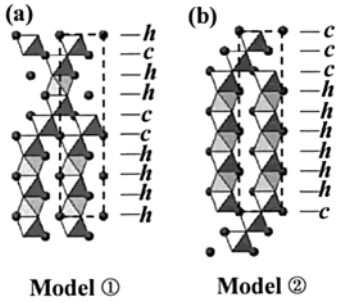

Figure 3. [100] projection of the ideal structure models (a) 1 and (b) 2.

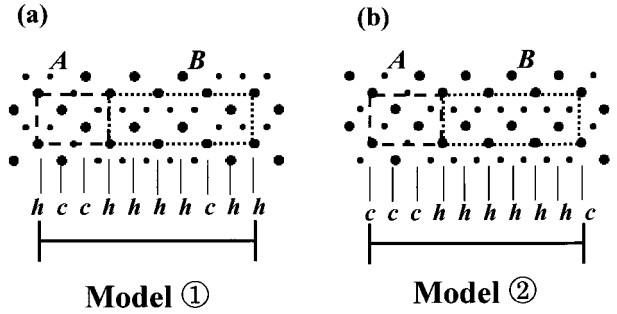

Figure 4. Schematic representation of blocks constituting (a) model 1 and (b) model 2.

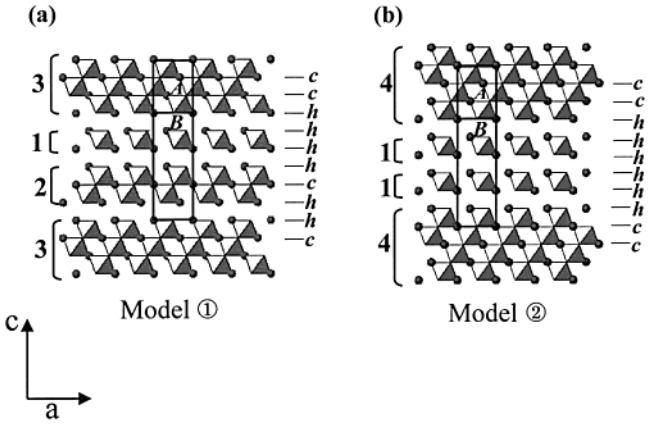

Figure 5. Ideal structure models projected along [100], showing the location of the cationic vacancies in (a) model 1 and (b) model 2.

parts a and b of Figure 4 for models 1 and 2, respectively. From the drawings, it can be appreciated that block A should correspond to the same array of bright dots in both cases although the first *h* layer changes to *c* when considering model 2 instead of model 1. Block B, however, has different layer sequence in 1 and 2; it is constituted by four *h* layers separated by one *c* layer from other two *h* layers in model 1, while the six *h* layers constitute a unique block in model 2.

Because of the actual composition, in particular to the cation deficiency, not all octahedral interstices can be occupied. As previously shown,[6,7] the niobium deficiency is usually accommodated as complete layers of vacant octahedral interstices, and these layers are located in the midplanes of the quadruplets of layers resulting from every two adjacent hexagonally stacked triplets. In the present case, there is one cationic vacancy per formula, i.e., three empty sites per unit cell. To ensure the largest separation between B cations, location of cationic vacancies might be in models 1 and 2 as has been drawn in Figure 5, both arrangements reducing the electrostatic cationic repulsions.

From this representation, the two sequences can be described as consisting of blocks of different thicknesses with structure derived from that of cubic perovskite by introducing periodically intrinsic faults with a displacement vector 1/3[110] in the cubic stacking of close packed BaO_3 layers. The so-called intrinsic faults are the layers of vacant octahedral sites. Thus, model 1 is constituted by a 321 block sequence and model 2 by a 411 block sequence, where numbers refer to block thickness in terms of layers of octahedral sites.

Figure 6 shows in a comparative way the calculated images for both models.[8] The observation of the calculated images reveals the layers of octahedral empty sites appearing as dark lines (marked with arrows), thus dividing the bright dots sequences into blocks of 432 for model 1 and 522 in model 2. It can be seen the occurrence of the empty cationic layers inside the so-called block B of the unit cell. In the experimental

(6) Van Tendeloo, G.; Amelinckx, S.; Darriet, B.; Bontchev, R.; Darriet, J.; Weil, F. *J. Solid State Chem.* **1994**, *108*, 314.
(7) Shpanchenko, R. V.; Nistor, L.; Van Tendeloo, G.; Van Landuyt, J.; Amelinckx, S.; Abakumov, A. M.; Antipov, E. V.; Kovba, L. M. *J. Solid State Chem.* **1995**, *114*, 560.

(8) "Mac Tempas" software package.

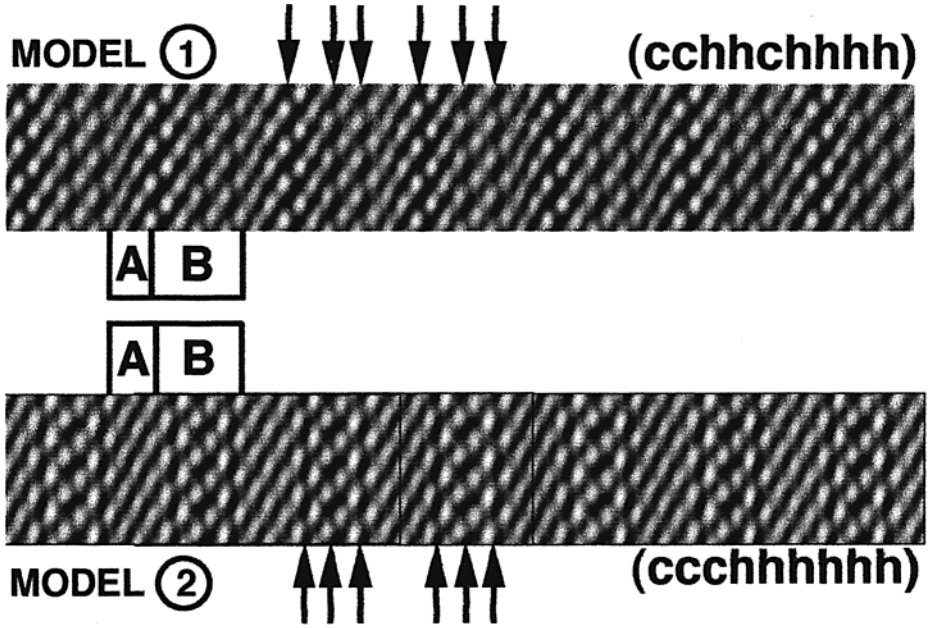

Figure 6. Calculated images in the [100] projection using the ideal atomic coordinates for *P*3*m*1 *(cchhchhhh)* (conditions: $\Delta f = -70$ nm, $t = 3$ nm) and *P*3*m*1 *(ccchhhhhh)* (conditions: $\Delta f = -70$ nm, $t = 3$ nm). Black arrows have been drawn to locate the cationic vacancy planes.

image, the dark fringes associated with the cationic defect layers are also located in the same block, which is likely to occur since it contains all the *h* layers constituting the unit cell. Both calculated and experimental images show, in the *cch* fragment of the unit cell (corresponding to the A block), the contrast to be homogeneously bright. In every case dark fringes appear at both sides of this central frame; they are distributed, in the simulated images, as leading to the 432 and 522 dots block sequences, respectively. The experimental image, however, does not reveal clearly the disposition of the vacant layers, and therefore it makes difficult to decide whether model 1 or model 2 fits better with the microstructural features of $Ba_3Nb_2O_8$. It is a fact that the intercalation of one cubic layer in a sequence constituted by six hexagonal layers gives rise to a very slight slope change in the contrast. Besides, we should take into account two more considerations. In first place, the actual anionic composition implies one vacancy per unit cell, and this fact has not been considered in the above discussion. Moreover, the atomic positions used as input data for the calculations performed are the atomic coordinates corresponding to the ideal models proposed and accurate atomic coordinates cannot be extracted from HREM image matching. Attempts to refine the metallic positions by powder X-ray diffraction data were not satisfactory, and we will make reference to it below. In addition, the thickness of the crystallites increases very quickly from their edge, producing dramatical changes in the image contrast and thus difficulting the images interpretation.

Therefore, emphasis has to be done in the fact that the distribution of white dots (i.e., the metallic atoms) inside the unit cell can be identified with any of the two proposed models because it is determined mainly by the layers stacking sequence, and they both only differ in one *c* layer as previously seen. However, the ensemble of facts influencing the contrast change in an experimental image and outlined above hinders the choice between the two proposed models.

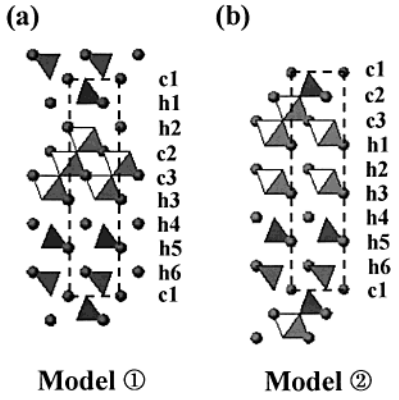

Figure 7. Ideal structure models projected along [100] showing the most probable distribution of anionic vacancies for (a) model 1 and (b) model 2.

As we have mentioned in the Experimental Section, the thermogravimetric analysis confirms the anionic composition to be O_8. This oxygen content would imply, if ordered, either three layers of composition BaO_2 and six BaO_3 or one BaO and one BaO_2 layers in addition to seven BaO_3 layers. One BaO layer corresponds to an anionic deficient hexagonal layer which generates two corner-sharing tetrahedra. One BaO_2 layer is an oxygen-deficient cubic layer which leads to two isolated tetrahedra.

From the stacking sequences of the proposed models, the presence of three BaO_2 layers to accommodate the oxygen composition is not possible topologically speaking. Therefore, the ensemble of one BaO, one BaO_2, and seven BaO_3 layers leads in both models 1 and 2 to a 1:1 ratio of octahedrally and tetrahedrally coordinated Nb atoms, although ordered in different disposition. As can be observed in Figure 7, this ordered location of the anionic vacancies is neccessarily associated with the ordered distribution of metallic atoms. In model 1, a *(hhc)* palmierite block is hexagonally stacked through a layer of vacant octahedral sites to a block constituted

by three layers of occupied octahedral sites if oxygen vacancies are placed at layers *c1* and *h4* and to a block constituted by two octahedral layers, if anionic vacancies are located at *c3* and *h5*. In model 2, the *(hhc)* block is separated through a layer of isolated octahedra from a block constituted by two layers of octahedrally coordinated Nb atoms, the three elements on a hexagonal disposition.

It would be equally possible to locate the BaO layer in any of the hexagonal layers as well as the BaO_2 layer in the place of the cubic layers. However, at this point we should take into account the study we have recently performed by means of Raman scattering;[9] the spectrum of $Ba_3Nb_2O_8$ has been registered in comparison to those of other 3:2 compounds. It beared strong similarity to that of $O_{8.5}$ anionic composition where vibrational modes of octahedrally coordinated BO_6 groups become evident as a consequence of the fact that the structural framework of the palmierite structure is preserved, but 50% of tetrahedra change to octahedra.[2] Thus, in agreement with the Raman scattering results, the presence of both octahedrally and tetrahedrally coordinated Nb is corroborated for $Ba_3Nb_2O_8$ even though the anionic composition is the same as that of the palmierite compounds. At the same time the presence of palmierite blocks in this structure can be deduced. We have to mention that the formation of an octahedral environment for the Nb atoms in the structure of the $Ba_3Nb_2O_8$ compound is consistent with the fact that Nb(V) ions seldom occur in tetrahedral coordination, in contrast to V(V) which is preferentially placed in tetrahedral sites.

Therefore, from the above discussion, it seems reasonable to propose the models shown in Figure 7 as the most probable ordered distribution of anionic vacancies in the two possible 9H stacking sequences.

Partial order of the anionic deficiency inside only one type of layer (*c* or *h*) would be also possible, and it should be related to the partially ordered distribution of the cationic vacancies. Then although both models a and b in Figure 7 can accommodate the nominal composition, the presence of more than two consecutive hexagonal layers is probably associated with some cationic vacancy disorder. This fact would imply certain fractional occupation of every octahedron in the blocks, which is more likely to occur if we take into account the impossibility in getting satisfactory *R* factors by refinement of powder X-ray diffraction data, when considering any of the two structural models proposed. Attempts to distribute statistically the niobium vacancies inside the hexagonal blocks were equally unsuccessful. In this sense, the need of long cooling rates to obtain the final crystalline product (as explained in the Experimental Section) is in agreement with the difficulties in getting a fully ordered disposition of vacant and occupied octahedra if we consider the relatively long period of the *hh*... blocks existing in the two possible structural models.

From the above discussion, we can conclude that the $Ba_3Nb_2O_8$ phase does not present rhombohedral symmetry and therefore does not adopt the palmierite structure as previously reported. The symmetry changes to hexagonal correspond to a 9H type. Microstructural characterization by means of HREM allows us to propose only two polytypes from the six possible 9H sequences, but it cannot be established whether one or the other is adopted. In fact, some fractional occupation of every cationic polyhedra must probably occur, and in that case, an intermediate situation between the two models would be the more realistic description.

Acknowledgment. We are grateful to the Centro de Microscopía Electrónica (UCM) for facilities. We acknowledge finantial support of CICYT (Spain) through Project MAT98-0648.

CM000007F

(9) Brown Holden A. A.; Reedyk, M.; García-González, E.; Parras, M.; González-Calbet, J. M. *Chem. Mater.*, in press.